CHAPTER 1

INTRODUCTION

During the last decade, research works in materials chemistry have principally focused on the synthesis of new compounds particularly those possessing multi-functionalities [1]. Along this line, the as-called inorganic–organic hybrid compounds (IOHs) have captured wide interest among the materials chemists. They are the compounds composing of both inorganic and organic components combined in molecular level. By incorporating inorganic and organic counterparts into a single structure, the IOHs can exhibit properties of both components [2]. The inorganic components generally provide the mainframes and some important physical properties such as magnetic and electric properties [3-6], while the organic components are the origin for various chemical functionalities [3]. During the fabrication of the IOH structures, the organic components can also direct the registry of the inorganic structures *via* various inorganic-organic interface interactions, for example, coordinate covalent bond, hydrogen bond, hydrophobic-hydrophilic interaction and ionic interaction [7].

Referring to definition of the IOHs, a large variety of compounds may be included. One of the most studied subjects nonetheless is polyoxovanadates (POVs) because of their potential uses in a wide range of applications [3] and the richness in their coordination and structural chemistry [5-7]. The magnetochemistry of POVs is also intriguing and still a subject of current interest, owing to the nature of vanadium

atoms that can adopt various oxidation states, and can be either fully or partially oxidized and reduced [8].

The synthesis of POVs however holds a key to open a door to the success. A common problem hindering the successful synthesis is the difficulties in predicting the exact nature of the final structures, which are due to (1) different dimensionality and structure that can be adopted by POVs, (2) different types of feasible metal-organic molecules interactions, and (3) functions of the organic molecules [1]. Consequently, the possibility in preparing POVs with rational design remains elusive. The knowledge on the synthesis as well as the influences of structure directing function of the organic molecules on the POV structures is therefore being both attractive and essential issue.

1.1 Structural Chemistry of Polyoxovanadates

Polyoxovanadates (POVs) or vanadium oxides have captured great interest from materials chemists because of their potential electronic and magnetic applications as well as their diverse structures and coordination chemistry [3,9]. These are due to the characteristics of vanadium atoms that can exhibit a wide range of oxidation states - V^{II} to V^{V} [3, 9] - and coordination geometries - regular tetrahedron, square pyramid, distorted trigonal bipyramid, square bipyramid and distorted octahedron (Figure 1.1). The difference in oxidation states of vanadium is well reflected by different coordination environments which can be regarded as one of their structural characteristics that may be employed in rational design of POV structures [9]. In addition, the V–O–V bridging interactions commonly found in

POVs are rather flexible, resulting in several possible inter-polyhedral linkage patterns [3]. Under mild reducing condition due to the presence of organic molecules generally used in the preparation of POVs under hydrothermal conditions, only two oxidation states namely V^{IV} and V^{V} are common [3]. The vanadium in POVs can be present in either only a single state of V^{IV} or V^{V}, or the mixing of the two, *i.e.* V^{IV}/V^{V}, in different degrees [10-12].For this reason; POVs are highly interesting for redox applications in catalysis and materials science [10-11].

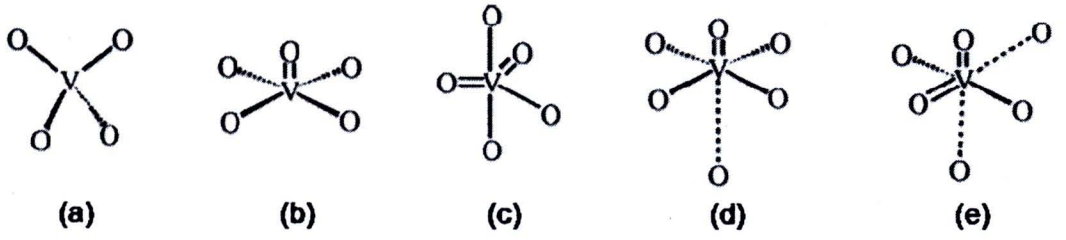

Figure 1.1 Feasible coordination geometries manifested by vanadium of different valences in POVs; (a) regular tetrahedron, (b) square pyramid, (c) distorted trigonal bipyramid, (d) square bipyramid and (e) distorted octahedron [3].

The popular approach adopted at the present for the synthesis of new IOHs is the incorporation of the secondary metal into the frameworks, as either part of the frameworks or the extra-framework units. This approach has been proved to be powerful in modifying the IOH structures and in fabricating novel IOHs [13-17]. The secondary metals may serve one of two following functions [18]; (1) being a linker adjoining the low dimensional IOH frameworks through either direct bonding (Figure 1.2a and Figure 1.2b) or π-π interaction of the organic ligands (Figure 1.2c) to give higher dimensional structures, and (2) being a cationic scaffold whose void is

occupied by metal oxide anionic motifs (Figure 1.2d-Figure 1.2f). In case of POVs, it may be worth noted that the secondary metals are present solely as the bridging units through either direct coordination or π-π interaction.

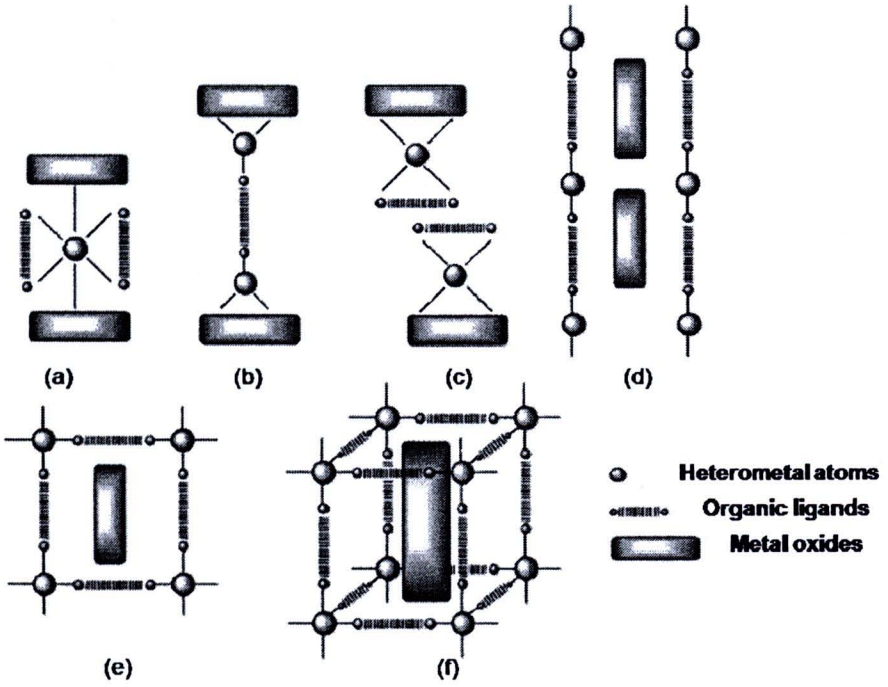

Figure 1.2 Schematic representations of different functions of the secondary metal-organic units [18].

According to literatures reported on the secondary metals-POV frameworks (M-POVs) as summarized in Figure 1.3 and Table 1.1, the secondary metals employed in the synthesis of POVs are usually the first row transition metals among which copper, zinc and nickel are the first three frequent used metals. It should be noted here that the survey was conducted using the following keywords - polyoxovanadate and vanadium oxide - in the following databases - SciFinder, Science direct and American Chemical Society. The search resulted in 79 structures reported during 1997-2007. Nickel has been chosen as the metal of interest in this

work because of its lability, rich coordination geometries and magnetic properties, as well as a large number of possible and facile reaction paths that can fortify the synthesis [38]. Regarding the previously reported structures of Ni-POVs, it is apparent that nickel almost always acts as a bridging unit linking low dimensional POVs to form the higher dimensional structures through direct coordinate covalent bonding [24-25, 27-28, 39-40]. If dimensionalities of the M-POV frameworks are considered, the outnumbering of the high dimensional frameworks to the zero dimensional ones is lucid (Figure 1.4). This is particularly true for the Ni-POVs, among which only one example of the zero dimensional framework has been reported, *i.e.* $Li_6[Ni^{II}_3(H_2O)_{12}V^{IV}_{16}V^{V}_2O_{42}(SO_4)]\cdot 24H_2O$ [8].

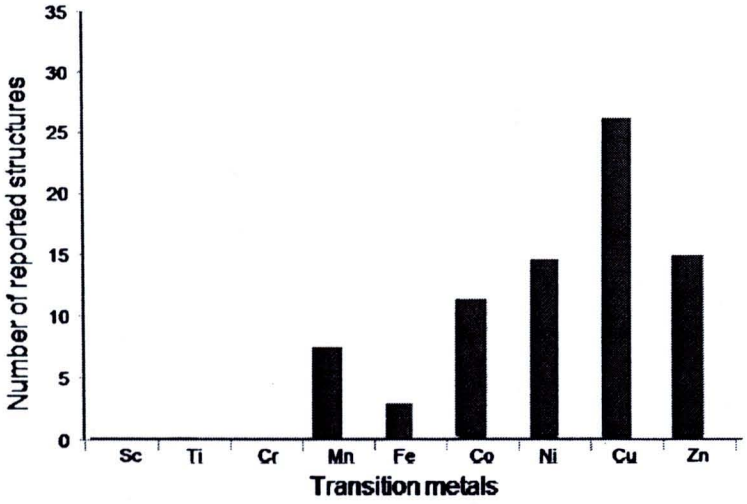

Figure 1.3 Number of M–POV structures reported during 1997-2007in SciFinder, Science direct and American Chemical Society [3, 8, 19-37; data retrieved on 12 December, 2008].

Table 1.1 List of previously reported M–POVs, where M is the first row transition metals, and their roles in the reported POV structures [3, 8, 19-37 data retrieved on 12 December, 2008].

Secondary metals	Compounds	Role	references
Mn	$[Mn^{II}_3(H_2O)_{12}H_6V^{IV}_{15}V^{V}_3O_{42}(V^{V}O_4)] \cdot 30H_2O$	bridging	[8]
	$Li_6[Mn^{II}_3(H_2O)_{12}V^{IV}_{16}V^{V}_2O_{42}(VO_4)]) \cdot 24H_2O$	bridging	[8]
	$Li_6[Mn^{II}_3(H_2O)_{12}V^{IV}_{16}V^{V}_2O_{42}(SO_4)]) \cdot 24H_2O$	bridging	[8]
	$(H_2en)[MnFV_3O_9]$	bridging	[8]
	$(H_2en)[Mn_3(H_2O)_2V_4O_{14}]$	bridging	[8]
	$(H_2en)_2[MnV_6O_{18}]$	bridging	[3]
Mn	$[Mn(Hen)_2V_4O_{12}$	bridging	[3]
Fe	$Li_6[Fe^{II}3(H_2O)_{12}V^{IV}_{15}V^{V}_3O_{42}(V^{V}O_4)]) \cdot 24H_2O$	bridging	[8]
	$Fe^{II}_3(H_2O)_{12}V_{18}O_{42}(VO_4)]) \cdot 24H_2O$	bridging	[8]
	$Fe^{II}_3(H_2O)_{12}V_{18}O_{42}(SO_4)]) \cdot 24H_2O$	bridging	[8]
Co	$(C_2H_{10}N_2)[Co_2(C_2O_4)V_4O_{12}]$	bridging	[19]
	$[\{Co(tpyprz)\}_2V_4O_{12}] \cdot 0.25H_2O$	bridging	[20]
	$[Co(phen)_3][V_{10}O_{26}] \cdot H_2O$	charge-compensating and space filling	[21]
	$[Co(bpy)]_2[V_{12}O_{32}]$	bridging	[22]
	$[\{Co(H_2O)_2\}V_2O_6]$	bridging	[23]
	$[Co(H_2O)(2,2'\text{-bpy})V_2O_6]$	bridging	[24]
	$[Co^{II}_3(H_2O)_{12}V_{18}O_{42}(VO_4)]) \cdot 24H_2O$	bridging	[8]
	$[Co^{II}_3(H_2O)_{12}V_{18}O_{42}(SO_4)]) \cdot 24H_2O$	bridging	[8]
	$[Co(Hdpa)_2V_4O_{12}]$	bridging	[3]
	$[\{Co(bpy)\}_2V_{12}O_{32}]$	bridging	[3]
	$[\{Co(3,3'\text{-bpy})\}_2V_4O_{12}]$	bridging	[3]
	$(Me_4N)_2[Co(H_2O)_4V_{12}O_{28}]$	bridging	[3]

Table 1.1 List of previously reported M–POVs, where M is the first row transition metals, and their roles in the reported POV structures [3, 8, 19-37] (continued).

Secondary metals	Compounds	Role	references
Co	$[\{Co(3,3'\text{-bpy})\}_2V_4O_{12}]$	bridging	[3]
	$(Me_4N)_2[Co(H_2O)_4V_{12}O_{28}]$	bridging	[3]
Ni	$[\{Ni(tpyprz)\}_2V_4O_{12}]\cdot 0.25H_2O$	bridging	[20]
	$[Ni(2,2'\text{-bpy})_2[V_{12}O_{32}]$	bridging	[22]
	$[\{Ni(H_2O)_2\}V_2O_6]$	bridging	[23]
	$[Ni(phen)_3]_2[V_4O_{12}]\cdot 17.5H_2O$	charge-compensating and space filling	[25]
	$Ni(NH_3)_2(VO_3)_2$	bridging	[26]
	$[Ni(H_2O)(2,2'\text{-bpy})V_2O_6]$	bridging	[24]
	$Li_6[Ni^{II}_3(H_2O)_{12}V^{IV}_{16}V^{V}_2O_{42}(SO_4)]\ )\cdot 24H_2O$	bridging	[8]
	$[Ni(en)_3][V_2O_6]$	bridging	[3]
	$[Ni(dien)V_2O_6]$	bridging	[3]
	$[Ni(Hdpa)_2V_4O_{12}]$	bridging	[3]
	$[\{Ni(bpy)\}_2V_{12}O_{32}]$	bridging	[3]
	$[Ni(en)_2V_6O_{14}]$	bridging	[3]
	$[Ni(en)_2]_{0.5}[V_3O_7]$	bridging	[27]
	$(H_2enMe)[Ni(en)_2V_{12}O_{28}]$	bridging	[3]
	$[Ni(enMe)_2]_{0.5}[H_2enMe]_{0.5}[V_6O_{14}]$	bridging	[27]
Cu	$[\{Cu_2(tpyprz)\}_2V_4O_{12}]\cdot 2H_2O$	bridging	[20]
	$[Cu(bpy)]_2[V_{12}O_{32}]$	bridging	[22]
	$Cu(en)_2[V_6O_{14}]$	bridging	[22]
	$[Cu(phen)V_4O_{10}]_\infty$	bridging	[28]

Table 1.1 List of previously reported M–POVs, where M is the first row transition metals, and their roles in the reported POV structures [3, 8, 19-37] (continued).

Secondary metals	Compounds	Role	references
Cu	$[Cu(2,2'\text{-bpy})V_4O_{10.5}]$	bridging	[31]
	$[Cu(terpy)V_2O_6]$	bridging	[31]
	$Cu(tn)_2(VO_3)_2$	charge-compensating	[28]
	$Na_2[CuV_2O_2(H_2O)_2(O_3PCH_2PO_3)_2]$	bridging	[30]
	$[Cu(en)_2]_2[V_{10}O_{25}]$	bridging	[3]
	β-$[Cu(bpy)V_2O_6]$	bridging	[3]
	$[Cu(bpy)_2V_2O_6]$	bridging	[3]
	$[Cu(prn)_2V_2O_6]$	bridging	[3]
	$[Cu(dien)V_2O_6]$	bridging	[3]
	α-$[Cu(terpy)V_2O_6]$	bridging	[3]
	α-$[Cu(bpy)V_2O_6]$	bridging	[3]
	$[Cu(dpa)VO_3]$	bridging	[3]
	$[Cu(en)V_2O_6]$	bridging	[3]
	β-$[Cu(terpy)V_2O_6]$	bridging	[3]
	$[\{Cu(bpy)\}_2V_{12}O_{32}]$	bridging	[3]
	$[\{Cu(bpy)\}_2V_8O_{21}]$	bridging	[3]
	$[Cu(NH_3)_2V_2O_6]$	bridging	[3]
	$[Cu_3(trz)_2V_4O_{12}]$	bridging	[3]
	$\{[Cu_4V_{13}^{IV}V_5^{V}O_{42}(NO_3)(C_3H_{10}N_2)_8]\cdot 10H_2O\}_n$	bridging	[31]
	$\{[Cu_4V_{12}^{IV}V_6^{V}O_{42}(SO_4)(C_3H_{10}N_2)_8]\cdot 10H_2O\}_n$	bridging	[31]
	$\{Cu(en)_2\}_4[V_{15}O_{36}Cl]\cdot 12H_2O$	charge-compensating	[32]
	$\{Cu(pn)_2\}_4[V_{18}O_{42}Cl]\cdot 12H_2O$	charge-compensating	[32]

Table 1.1 List of previously reported M–POVs, where M is the first row transition metals, and their roles in the reported POV structures [3, 8, 19-37] (continued).

Secondary metals	Compounds	Role	references
Zn	$[\{Zn_2(tpyprz)\}V_4O_{12}]$	bridging	[20]
	$[\{Zn(2,2'\text{-bpy})\}_2V_4O_{12}]$	bridging	[29]
	$[\{Zn(terpy)\}_2V_6O_{17}]$	bridging	[29]
	$(N_2H_5)_2[Zn^{II}{}_3(H_2O)_{12}V^{IV}{}_{12}V^{V}{}_6O_{42}(SO_4)]) \cdot 24H_2O$	bridging	[8]
	$[Zn(en)_2][V_6O_{14}]$	bridging	[3]
	$[\{Zn(bpy)\}_2V_4O_{12}]$	bridging	[3]
	$[\{Zn(bpy)_2\}_2V_6O_{17}]$	bridging	[3]
	$[\{Zn(terpy)\}_2V_6O_{17}]$	bridging	[3]
	$[\{Zn(phen)_2\}_2V_4O_{12}]$	bridging	[3]
	$[Zn_3V_2O_7(OH)_2]\cdot 2H_2O$	bridging	[33]
	$[Zn(H_2O)_6][Zn_2V_{10}O_{28}(H_2O)_{10}]$	charge-compensating and space filling	[34]
	$[Zn_2(H_2N(CH_2)_2NH_2)_5[\{Zn(H_2N(CH_2)_2NH_2)_2\}_2V_{18}O_{42}(H_2O)]\cdot 9H_2O$	bridging	[35]
	$[Zn_2(H_2N(CH_2)_2NH_2)_5][Zn(H_2N(CH_2)_2NH_2)_2[V_{18}O_{42}(Cl)]\cdot 9H_2O$	bridging	[35]
	$[\{Zn(bpy)_2\}_2V_4O_{12}]$	bridging	[36]
	$[\{Zn(phen)_2\}_2V_4O_{12}]\cdot H_2O$	bridging	[36]
	$[Zn_2(NH_2(CH_2)_2NH_2)_5][\{Zn(NH_2(CH_2)_2NH_2)_2\}_2\{V_{18}O_{42}(H_2O)\}]\cdot H_2O$ (x ~ 12)	bridging	[37]

Reckoning the numbers of vanadium atoms present in the reported POVs, they are distributed in rather a wide range, *i.e.* 3-34 atoms per formula. However, only the high nuclearity POVs have been structurally characterized and reported (Figure 1.5). In the case of zero-dimensional clusters, only a large number of vanadium atoms, *i.e.* 15 atoms per formula, are usually found.

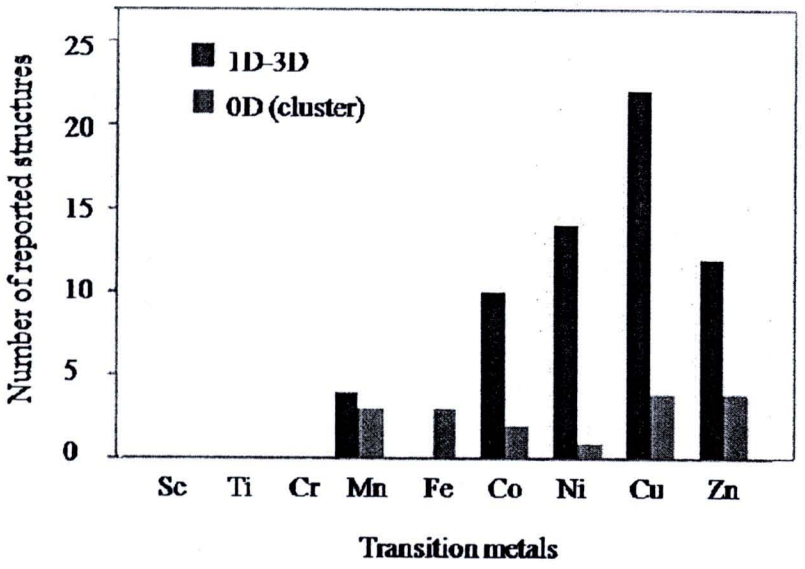

Figure 1.4 Numbers of M–POV structures reported during 1997-2007 in SciFinder, Science direct and American Chemical Society, classified by dimensionalities of the M–POVs [3, 8, 19-37].

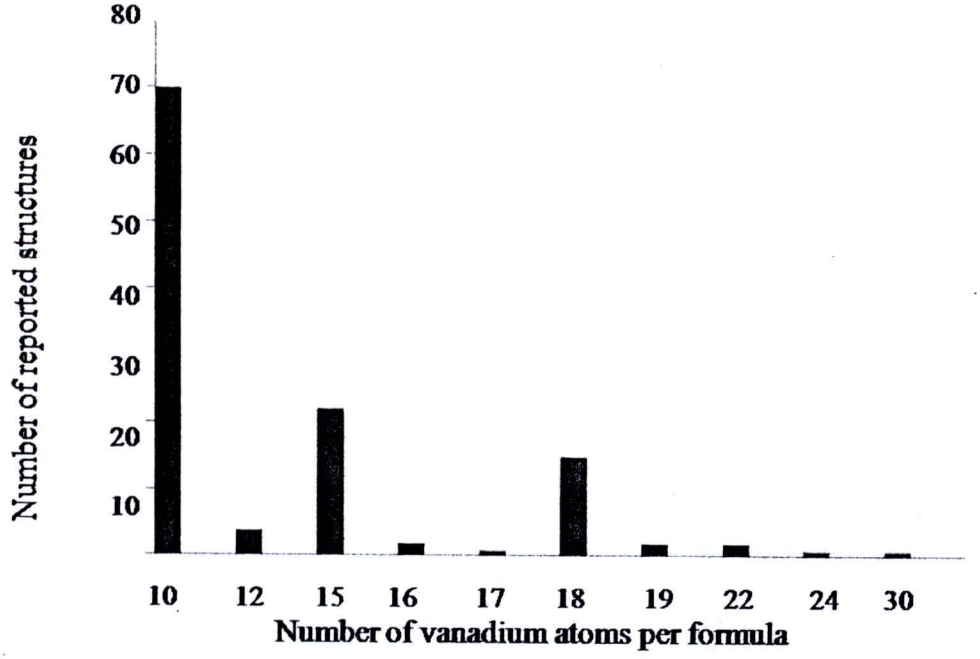

Figure 1.5 An overview of high nuclearity POVs [33].

As for the cluster cases, the V–O–V bridging interactions are flexible, resulting in a large number of possible POVs of high nuclearity (Figure 1.6). In the void of these clusters, there commonly located an encapsulated anion, *e.g.* Cl^- [32, 41], Br^- [36, 42], I^- [42], NO_2^- [8], SH^- [8], SO_4^{2-}[14], $HCOO^-$ [8], or small neutral species such as H_2O [12]. Different encapsulated species generally result in different shapes and therefore symmetries of the clusters, from which their template function is illustrated. For example, the $\{V_{18}O_{42}\}$ cluster shows the D_{4d} symmetry when the encapsulated species is H_2O ($\{V_{18}O_{42}(H_2O)\}^{12-}$), but the D_{2h} when the encapsulated species is changed to N_3^- ($\{V_{18}O_{44}(N_3)\}^{11-}$) [12].

The template function of the encapsulated species is believed to occur *via* the condensation reactions [43]. These clusters are assumingly formed from the $\{VO(OH)_4(OH_2)\}^-$ precursor of which one water molecule lies along the *z*-axis opposite to the short vanadyl V=O bond (Figure 1.7). The condensation reaction cannot proceed along this direction as there is no available V-OH group. It can therefore occur only in the *xy*-plane, where four V-OH bonds are present. These results in the formation of $[VO_5]$ square pyramids, which can link to each other *via* the corner or edge [44]. The condensation reaction as described will lead to the formation of two dimensional POV layers. The presence of the templating species may curve change the linking $[VO_5]$ units *via* the interaction between negative anions $X^-$and the positive vanadium atom ($V^{\delta+}$) [43]. All V=O dipoles are oriented toward the outside of the shell where they repel each other, favoring the formation of convex surface [44].

Among the high nuclearity POV clusters, defined by a number of vanadium atoms, the $\{V_{18}O_{42}\}$ is an important species because of its ability to form mixed-

valence species containing both V^{IV} and V^{V} in the same clusters [8, 42, 46], *e.g.* $\{V^{IV}_{18}O_{42}\}$ [8, 12], $\{V^{IV}_{16}V^{V}_{2}O_{42}\}$ [8, 14], $\{V^{IV}_{15}V^{V}_{3}O_{42}\}$ [42, 46], $\{V^{IV}_{14}V^{V}_{4}O_{42}\}$ [47], $\{V^{IV}_{13}V^{V}_{5}O_{42}\}$ [32], $\{V^{IV}_{12}V^{V}_{6}O_{42}\}$ [32, 46, 48], $\{V^{IV}_{10}V^{V}_{8}O_{42}\}$ [8]. These clusters are interesting due to the inherent luminescence properties, affording the compounds to be active in photo-oxidation reactions and therefore a potential photocatalyst [42, 45].

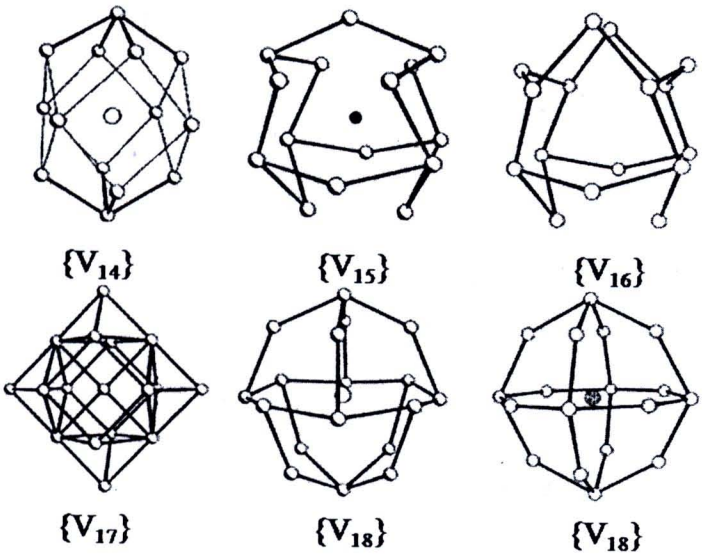

Figure 1.6 Examples of V-O-V linkage in POV clusters resulting in different numbers of involving vanadium atoms in the clusters [45].

The presence and absence of *d*-electron; d^1 for V^{IV} and d^0 for V^{V}, result in the diversified magnetochemistry of the V^{IV}/V^{V} systems. The magnetic interactions in these V^{IV}/V^{V}-POVs can be either anti-ferromagnetic or ferromagnetic, the former of which is the most abundant [8]. The magnetic properties of the V^{IV}/V^{V}-POVs can even be further complex when the structures of POVs are of the cluster type where the V-O-V bonds are curved [45], and the number of V^{IV}/V^{V} is varied. For example, the $\{V^{IV}_{16}V^{V}_{2}O_{42}\}$ cluster has $\chi_M T$ (260 K) of *ca.* 1.9 - 2.4 emu·K·mol^{-1}, while the $\chi_M T$

(260 K) for the $\{V^{IV}_{10}V^{V}_{8}O_{42}\}$ cluster is significantly lower, *i.e.* 0.9 emu·K·mol^{-1}. The magnetic coupling in both clusters is nonetheless alike, which is antiferromagnetic [8].

The $\{V_{18}O_{42}\}$ cluster is generally constructed from eighteen $[VO_5]$ square pyramids sharing the common edges through twenty four μ_3-oxygen atoms (Figure 1.8). All the $[VO_5]$ units comprise of a terminal vanadyl V=O and four μ_3-oxygen atoms [33]. The crystal structure analyses of the compounds show that the $\{V_{18}O_{42}\}$ cluster can exist in two different but closely related structural forms differentiated by the arrangement of the 24 μ_3-oxygen atoms in the cluster. The first one is a distorted rhombicuboctahedron (T_d) and the other is pseudorhombicuboctahedron (D_{4d}) (Figure 1.9). The D_{4d} form can be generated by rotating one-half of the rhombicuboctahedron for 45°about the S_4 axes [8, 14]. The $\{V_{18}O_{42}\}$ cluster with D_{4d} symmetry is the preference when relatively small and/or only slightly charged anions (monoanions like the halide anions) or small neutral molecules are employed [8].

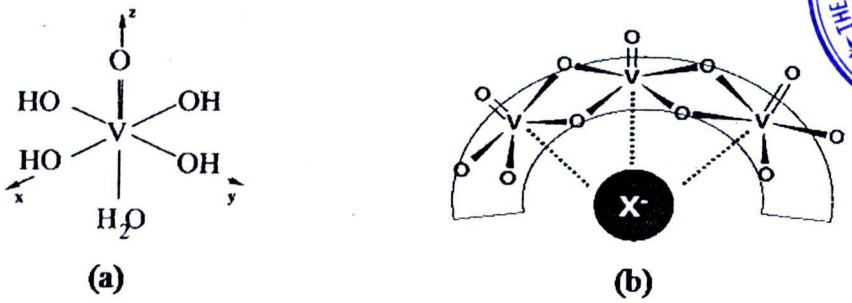

Figure 1.7 (a) The anionic $\{VO(OH)_4(OH_2)\}^-$ precursor [43, 44] and (b) the template function of the X^- anion [44].

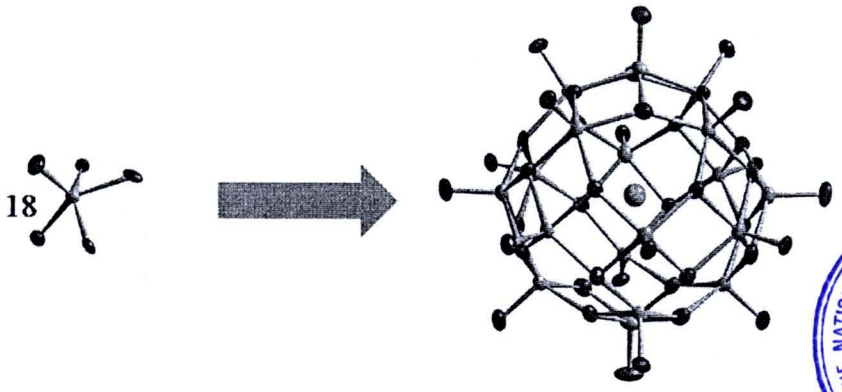

Figure 1.8 Depiction of the basic composition of $\{V_{18}O_{42}\}$ clusters [48].

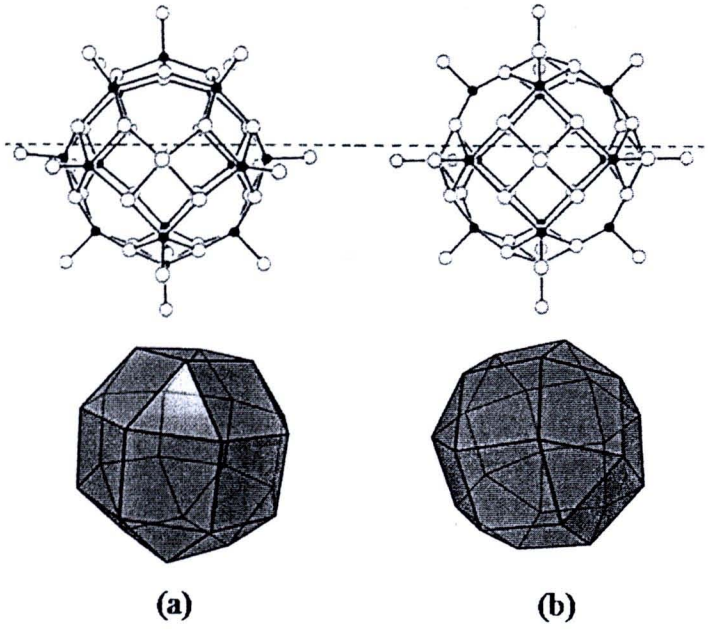

Figure 1.9 Depiction of the $\{V_{18}O_{42}\}$ cluster in (a) rhombicuboctahedron and (b) pseudorhombicuboctahedron [8].

In this research, the synthesis of new Ni-POVs of the cluster type will be attempted using the anionic template approach. The influences of various anions, and halides in particular, on Ni-POV structures will be elucidated.

1.2 Magnetism of POV clusters

The POV clusters exhibit unique magnetic behavior which is increasingly interesting in the last decade after it has been revealed that some of these clusters can indeed behave like tiny magnets [49]. However, the complete interpretation of the magnetism of the POV clusters until recently was not available particularly for those high nuclearities such as $\{V_{18}O_{42}\}$ [49]. The magnetic properties of this cluster have been investigated but a number of the well-characterized complexes were small, and no detailed conclusion could be reached because of the insufficiency in structural and/or magnetic data [49]. This deficiency may be due to the complexities in the structures of the POV clusters especially for $\{V_{18}O_{42}\}$ [8], where the V-O-V bonds are curved, and the number of V^{IV}/V^{V} can be varied. Until in the more recent years, the analysis of the magnetic coupling phenomena in three types of $\{V_{18}O_{42}\}$, including $\{V^{IV}{}_{18}O_{42}\}$, $\{V^{IV}{}_{16}V^{V}{}_{2}O_{42}\}$ and $\{V^{IV}{}_{10}V^{V}{}_{8}O_{42}\}$, was reported. In the simplest case of $\{V^{IV}{}_{18}O_{42}\}$ clusters, the average effective magnetic moment at high temperature is 1.2 μ_B/V^{IV} which is much lower than the expected value of 1.7 μ_B/V^{IV} for the uncoupled spins. This indicated an overall antiferromagnetic coupling. The temperature dependence of $\chi_M T$ is shown in Figure 1.10.

The $\chi_M T$ values decrease on lowering temperature. These results show a marked decrease of slope around 40 K and a much faster decrease at 15 K, with $\chi_M T$ approaching 0.4 emumol^{-1}K at 2.8 K. In case of $\{V^{IV}_{16}V^{V}_{2}O_{42}\}$ and $\{V^{IV}_{10}V^{V}_{8}O_{42}\}$, the temperature dependence of $\chi_M T$ is quite similar to the results of the $\{V^{IV}_{18}O_{42}\}$ clusters. However, the explanation of the magnetic properties in cases of mixed-valence clusters, *i.e.* $\{V^{IV}_{16}V^{V}_{2}O_{42}\}$ and $\{V^{IV}_{10}V^{V}_{8}O_{42}\}$, is more complicated. The average effective magnetic moment at room temperature per V^{IV} center is 1.0 μ_B for the $\{V^{IV}_{16}V^{V}_{2}O_{42}\}$ and around 0.8 μ_B for the $\{V^{IV}_{10}V^{V}_{8}O_{42}\}$.

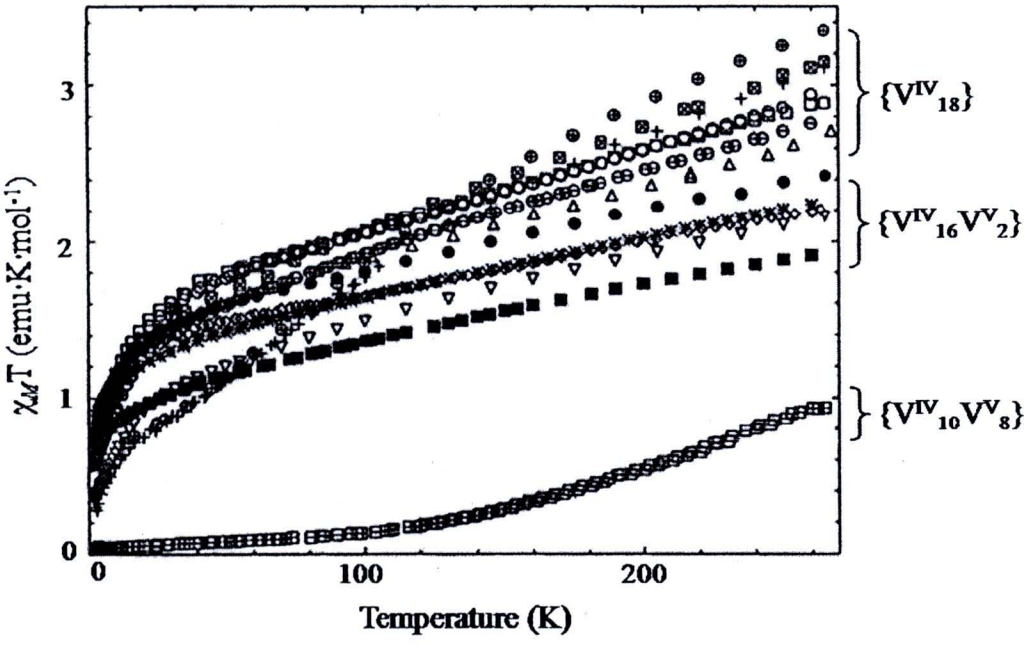

Figure 1.10 Temperature-dependence of $\chi_M T$ for various $\{V_{18}O_{42}\}$ clusters [8].

These results can be compared with the value of 1.2 μ_B reported for the $\{V^{IV}_{18}O_{42}\}$ clusters. According to these data, the antiferromagnetic coupling is larger in the clusters comprising smaller numbers of magnetic V^{IV} centers, while the effective interactions are weak on increasing the number of diamagnetic V^{V} ions. This

agrees with the temperature dependence of the magnetic susceptibility of the clusters, which shows that the $\{V^{IV}_{10}V^{V}_{8}O_{42}\}$ becomes diamagnetic at relatively high temperatures, while the other two types of clusters, $\{V^{IV}_{18}O_{42}\}$ and $\{V^{IV}_{16}V^{V}_{2}O_{42}\}$, require lower temperatures [8]. A quantitative analysis of $\{V_{18}O_{42}\}$ clusters is also difficult because the overall states which need to be considered are superabundant and thus it requires long time of calculation. Therefore, it seems to be rather satisfactory that indeed the magnetic properties of relatively large clusters can at least be semi-quantitatively interpreted, using parameters which compare well with those obtained from the analysis of simpler clusters [49].

1.3 Determination of Degree of Valence Mixing in V^{IV}/V^{V}-POVs

The method that is usually employed in defining the oxidation state of an interesting atom for crystal chemists is the bond valence sum calculation [8, 45], which has been developed from the second rule of Pauling; the charge (valence) *Vj* of ions has a propensity to be compensated with the valence strengths (s_{ij}) of the ions coordinated to the given ion ($Vj = \Sigma s_{ij}$) [50]. This directly concerns with chemical bonds, of which bond strength are reciprocally related to bond distance. The strength of bonding can therefore be determined from bond distances through the following one parameter model equation:

$$s_{ij} = \exp\left[\frac{\left(R_0 - R_{ij}\right)}{b}\right] \qquad (1.2.1)$$

where, R_{ij} = related bond distances

R_0 = bond valence parameter (the bond length having a bond valence of 1)

b = the characteristic parameter of particular bond

Since the bond strength also depends on the oxidation state of atom, the lengths of the coordinated bonds can also be used to calculate the oxidation state of the center atom [50-51].

$$V_j = \sum_{i=1}^{N} \exp\left[\frac{(R_0 - R_{ij})}{b}\right] \quad (1.2.2)$$

In the case of $\{V_{18}O_{42}\}$ clusters, the bond valence sum calculation is however not popular. According to the literatures survey, there is only one example reported by Muller *et.al.*, reporting the bond valence calculation of three $\{V_{18}O_{42}\}$ clusters including $\{V^{IV}{}_{18}O_{42}\}$, $\{V^{IV}{}_{16}V^{V}{}_{2}O_{42}\}$ and $\{V^{IV}{}_{10}V^{V}{}_{8}O_{42}\}$, as summarized in Table 1.2 [8]. It should be noted that these data are of the naked vanadium clusters. The oxidation states of vanadium atoms have been calculated using equation 1.3.2 using the empirical R_0 = 1.890 Å and b = 0.314. In fact, the other values of R_0 and b are also available, *i.e.* R_0 = 1.803 and 1.784 Å for V^V and V^{IV} sites, respectively and b = 0.37 [47, 52].

The oxidation states of vanadium atoms in POV clusters can be determined by other methods, including manganometric titration [8, 14, 46, 47], where the number of the reduced vanadium (V^{IV}) atoms per formula unit is determined by titrating their acidic solutions against standardized $KMnO_4$ solution [46, 47]. In case of POVs,

although the compounds contain both V^{IV} and V^{V}, only V^{IV} react with MnO_4^-. The possibly related equations are shown.

$$VO_2^+ + 2H^+ + e^- \rightarrow VO^{2+} + H_2O \qquad E^0 = 1.00\ v$$

$$MnO_4^- + 8H^+ + 5e^- \rightarrow Mn^{2+} + 4H_2O \qquad E^0 = 1.49\ v$$

$$MnO_4^- + 5VO^{2+} + H_2O \rightarrow Mn^{2+} + 5VO_2^+ + 2H^+$$

Table 1.2 Bond valence sum for the $\{V_{18}O_{42}\}$ clusters [8].

Cluster type	Compounds	bond valence calculations	average bond valence calculations
$\{V^{IV}_{18}O_{42}\}$	$Cs_{12}[V^{IV}_{18}O_{42}(H_2O)]\cdot 14H_2O$	3.83-4.27	4.07
	$K_{12}[V^{IV}_{18}O_{42}(H_2O)]\cdot 16H_2O$	4.01-4.32	4.12
	$Rb_{12}[V^{IV}_{18}O_{42}(H_2O)]\cdot 19H_2O$	4.01-4.34	4.17
	$K_9[H_3V^{IV}_{18}O_{42}(H_2O)]\cdot 14H_2O\cdot 4N_2H_4$	4.06-4.10	4.08
	$K_{11}[H_2V^{IV}_{18}O_{42}(Cl)]\cdot 13H_2O\cdot 2N_2H_4$	4.08-4.42	4.19
	$K_9[H_4V^{IV}_{18}O_{42}(Br)]\cdot 14H_2O\cdot 4N_2H_4$	4.14-4.38	4.23
	$K_9[H_4V^{IV}_{18}O_{42}(I)]\cdot 14H_2O\cdot 4N_2H_4$	3.92-4.21	4.12
	$K_{10}[H_3V^{IV}_{18}O_{42}(Br)]\cdot 13H_2O\cdot 0.5N_2H_4$	4.07-4.32	4.16
	$K_9[H_4V^{IV}_{18}O_{42}(NO_2)]\cdot 14H_2O\cdot 4N_2H_4$	4.11-4.31	4.21
	$Cs_{11}[H_2V^{IV}_{18}O_{42}(SH)]\cdot 12H_2O$	4.10-4.37	4.19
$\{V^{IV}_{16}V^{V}_{2}O_{42}\}$	$K_{10}[HV^{IV}_{16}V^{V}_{2}O_{42}(Cl)]\cdot 16H_2O$	4.17-4.53	4.32
	$Cs_9[H_2V^{IV}_{16}V^{V}_{2}O_{42}(Br)]\cdot 12H_2O$	4.18-4.50	4.37
	$K_{10}[HV^{IV}_{16}V^{V}_{2}O_{42}(Br)]\cdot 16H_2O$	4.10-4.44	4.25
	$K_{10}[HV^{IV}_{16}V^{V}_{2}O_{42}(I)]\cdot 16H_2O$	4.12-4.49	4.27
	$Cs_9[H_2V^{IV}_{16}V^{V}_{2}O_{42}(I)]\cdot 12H_2O$	4.12-4.43	4.29
	$K_{10}[HV^{IV}_{16}V^{V}_{2}O_{42}(HCOO)]\cdot 15H_2O$	4.08-4.65	4.24
	$Na_6[H_7V^{IV}_{16}V^{V}_{2}O_{42}(VO_4)]\cdot 21H_2O$	3.85-4.58	4.29
$\{V^{IV}_{10}V^{V}_{8}O_{42}\}$	$(NEt)_5[V^{IV}_{10}V^{V}_{8}O_{42}(I)]$	4.40-4.73	4.59

To elucidate number of V^{IV} atoms obtained by this titration method, the back titration with SO_2 which is generated from Na_2SO_3 needs to be performed to investigate the number of all vanadium atoms again as the following steps.

$$V^{V} \xrightarrow[\text{from } Na_2SO_3]{SO_2} V^{IV}$$

$$V^{IV} + MnO_4^- \rightarrow V^{V} + Mn^{2+}$$

Since the development of quantum chemistry and the emergence of computational chemistry, this semi-theoretical or theoretical approach have been employed in solving various problems in chemistry, *e.g.* transition states in chemical reaction and intermolecular force in various chemical systems. This approach can also be attempted in order to determine the valences of vanadium in POVs.

To evaluate electronic structure in quantum chemistry, there are three main approachess; semi-empirical, *ab* initio, and density-functional method [53]. Semi-empirical molecular quantum-mechanical methods use a simpler Hamiltonian than the correct molecular Hamiltonian and use parameters whose values are adjusted to fit experimental data or the results of *ab* initio calculations [54]. Semi-empirical calculations are relatively inexpensive and provide reasonable qualitative descriptions of molecular systems and fairly accurate quantitative predictions of energies and structures for systems where good parameter sets exist [53]. In contrast, *ab* initio calculation uses the correct Hamiltonian and does not use experimental data other than the values of the fundamental physical constants [54]. Moreover, *ab* initio computations provide high quality quantitative predictions for a broad range of

systems. Early *ab* initio programs were quite limited in the size of system they could handle. However, this is not true for modern *ab* initio programs.

Density-functional method or Density Functional Theory (DFT) is similar to *ab* initio methods in many ways. DFT calculations require about the same amount of computation resources as Hartree-Fock theory, the least expensive *ab* initio method [58].However, DFT does not attempt to calculate the molecular wave function but calculates the molecular electron probability density; p and calculates the molecular electronic energy from p that is why DFT have come into recently wide use [54]. DFT methods are attractive because they include the effects of electron correlation. That come from the fact that electrons in a molecular system react to one another's motion and attempt to keep out of one another's way. DFT methods compute electron correlation *via* general functional of the electron density.

The approximate functional employed by current DFT methods were proposed by Kohn and Sham. In Kohn–Sham equation, the total energy of a system is expressed as a functional of the charge density as

$$E[\rho] = T_s[\rho] + \int dr\, v_{ext}(r)\rho(r) + V_H[\rho] + E_{xc}[\rho] \qquad (1.3.1)$$

where T_s is the Kohn–Sham kinetic energy. v_{ext} is the external potential which is the electron-nuclei interaction for a molecular system. V_H is the Hartree (or Coulomb) energy, and E_{xc} is the exchange-correlation energy. The last term is the only unknowns in the Kohn–Sham approach to density functional theory [55]. A variety of functionals have been defined to identify this term, generally distinguished by the way that they treat the exchange and correlation components. The first one is *local*

exchange and correlation functionals that involve only the values of the electron spin densities. Another functional is *gradient-corrected functional* that involve both the values of the electron spin densities and their gradients that are accurate and efficient method for calculations involving *d*-metal complexes [56]. Such functional is also sometimes referred to as non-local in the literature.

A popular *gradient-corrected exchange functional* is one proposed by Becke in 1988; a widely-used *gradient-corrected correlation functional* is the LYP functional of Lee, Yang and Parr. The combination of the two forms the B-LYP method. Perdew has also proposed some important gradient-corrected correlation functionals, known as Perdew 86 and Perdew-Wang 91 [53] and the Perdew–Burke–Ernzerh of exchange-correlation potential (PBE) [57].

For vanadium oxide framework as well as polyoxovanadate clusters, quantum chemistry especially *ab* initio and DFT calculations were employed to study their properties with different objectives and methods. The structure and stability of small various clusters were determined by DFT with diverse calculations of BPW91/LANL2DZ [58], BP86 [59] and B3LYP [60]. For the theoretical study of larger vanadium oxide cluster; $V_{12}O_{32}$, the origin of the host-guest interaction energy were investigated by means of *ab* initio Hartree-Fock calculations [61]. However for the complex clusters, conventional *ab* initio cannot used to study properties of the structure because of the number of relevant parameters. Therefore the combination of *ab* initio calculations and the model Hamiltonian was applied to study the magnetic properties of a series of polyoxovananadate clusters of formula $\{V_{18}O_{42}\}^{12-}$ and $\{V_{18}O_{42}\}^{4-}$ [62].